ISIJ International, Vol. 38 (1998), No. 7, pp. 766–774

Continuous Cooling Transformation Behaviour of High Strength Microalloyed Steels for Linepipe Applications

P. A. MANOHAR and T. CHANDRA

Department of Materials Engineering, University of Wollongong, Northfields Avenue, Wollongong, NSW-2522, Australia.
E-mail: pam07@unow.edu.au

(Received on January 20, 1998; accepted in final form on March 20, 1998)

Continuous cooling transformation (CCT) behaviour of high strength microalloyed steels containing two different levels of Mn+Si additions is investigated in undeformed and thermomechanically processed conditions using quench and deformation dilatometry respectively. The deformation schedule used in the dilatometer is designed to simulate the industrial controlled rolling procedures for the production of plates as closely as possible in laboratory. CCT diagrams for the undeformed and thermomechanically processed steels are constructed. Effects of thermomechanical processing (TMP), accelerated cooling and composition (Mn+Si levels) on γ transformation start temperature (Ar_3), phase transformation kinetics, CCT diagrams and microhardness are investigated.

The results show that TMP accelerates the onset of γ/α transformation (Ar_3 is raised), but the progress of γ/α transformation is retarded considerably in deformed samples. Significant retardation is observed during the final 30% of the phase transformation reaction. Increase in cooling rate lowers the Ar_3 significantly and accelerates the progress of transformation. The steel with a higher level of Mn+Si addition (1.96%) exhibits lower Ar_3, sluggish transformation kinetics and higher hardnesses in undeformed and thermomechanically processed conditions as compared with the steel with a lower level of Mn+Si addition (1.17%). These effects are explained in terms of the effects of Mn and Si contents on the carbon partitioning and the subsequent phase transformation behaviour of these steels during continuous cooling. Increase in cooling rate increases the microhardnesses of both steels while TMP lowers them.

KEY WORDS: thermomechanical processing; microalloyed steels; dilatometry; CCT diagrams.

1. Introduction

Modern technology for the production of electric resistance welded (ERW) gas and oil pipeline steel is aiming to achieve quality welds in higher and higher strength steels. High strength line pipe steels (API X60 to X80) are produced through a judicious selection of (micro)alloy composition, and optimisation of thermomechanical processing (TMP) and accelerated cooling conditions subsequent to the TMP. The economic benefits of higher strength pipelines such as reduced gas transportation costs, lower pipe procurement and transport to the site costs and reduced welding costs due to smaller diameter and thinner wall are of critical importance where pipelines are to be laid over long distances.[1] Improvement in weldability, on the other hand, provides a challenging problem because weldability results from the combination of weld joint, welding procedures, welding technology and alloy composition and properties. However, from a metallurgical point of view, weldability includes hardenability, HAZ properties, HAZ and weld metal cracking and response of steels to post-weld heat treatments.[2] Improvement in weldability can be achieved through several metallurgical processes such as inclusion shape control (Ca, Ti, RE treatment), lowered S and P contents, improvement of steel making and continuous casting practices,[1] effective utilisation of TiN technology[3] (Ti content between 0.010–0.015%, and Ti : N ratio $\leq$3.42), and a reduction in C, Mn and Si contents to reduce segregation of these elements to the centreline during continuous casting and welding.[4] It has been shown by Williams *et al.*[1] that reduced Mn level reduces centreline microstructural banding resulting in low segregation ratio of hardenability enhancing Mn, which reduces considerably the potential for martensite formation in the hot rolled strip and plate. Taillard *et al.*[5] reported that Si content should be <0.1% to improve the toughness of intercritical and coarse grained HAZ (CGHAZ) in Ti-mictroalloyed steels. Lee and Pan[6] have suggested that reduction in Si content in Ti-microalloyed steels improves the toughness of HAZ by allowing the Ti to form TiO which is considered most effective in nucleating acicular ferrite microstructure which has a higher toughness than either allotrimorphic or widmanstatten ferrite.

In the present work, continuous cooling transformation (CCT) behaviour of two Ti-bearing microalloyed steels which are used in the manufacture of ERW line pipe is investigated. The steels contain two different levels of Mn+Si additions (1.97 and 1.17%) and thus possess

inherently different weldabilities. The purpose of the present investigation was to construct the CCT diagrams for the undeformed and thermomechanically processed steels using quench and deformation dilatometry respectively. CCT diagrams are believed to be useful not only in designing an optimum TMP and accelerated cooling schedule during industrial processing of these steels but also in gaining an insight into the microstructures of HAZ of ERW welds. The deformation schedule used in the dilatometer has been designed to simulate the industrial controlled rolling procedures for the production of plates as closely as possible in laboratory. The cooling rates chosen in this study are those encountered in practice during air cooling or accelerated cooling after plate rolling. Effects of thermomechanical processing (TMP), accelerated cooling and composition (Mn+Si levels) on γ transformation start temperature (Ar_3), phase transformation kinetics, CCT diagrams and microhardness are mainly investigated.

2. Materials

Chemical compositions of the steels studied are given in **Table 1**. Both steels were supplied in 220 mm thick continuous cast slab condition by BHP Steel Co., Port Kembla, Australia. Low-Mn+Si steel contains reduced levels of C, Mn and Si for improved weldability with a strength compensatory addition of slightly higher Nb content. Low-Mn+Si steel composition is designed for smaller diameter pipes (*e.g.* 273 and 219 mmϕ) produced from centre slit hot rolled coils. Experimental program used for constructing the CCT diagrams of above two steels is described in the following section.

3. Experimental Procedure

Specimens used for quench dilatometry (undeformed samples) were 10 mm long cylindrical tubes with an outside diameter of 5 mm and wall thickness of 0.75 mm while those for deformation dilatometry were 6 mm long solid cylinders of 3.2 mm in diameter. Thermocouple was spot welded on the surface of the samples during each test to continuously monitor sample temperature. 0.025 mm thick tantalum foils were spot welded on the contact surfaces of the deformation samples and boron nitride powder was used to minimise friction to promote homogeneous deformation. The tests were carried out in vacuum (10^{-4} torr). Cooling of the samples was achieved by controlling high purity He gas flow. Linear cooling rates of 0.3, 1, 3, 10, 30 and 50°C/s were employed to construct the CCT diagrams. Specimens were sectioned, mounted and prepared for metallographic examination

Table 1. Chemical composition of the steels studied. (Elements in wt% except N which is in ppm)

	C	Mn	Si	Al	Mo	Nb	Ti	N	CEQ*	P_{cm}†
Hi-Mn+Si	0.08	1.55	0.41	0.027	0.18	0.031	0.013	44	0.38	0.19
Low-Mn+Si	0.07	1.08	0.09	0.032	0.19	0.040	0.014	36	0.29	0.14

* Carbon equivalent (CEQ IIW) is calculated according to[7]:

$$CEQ = C + \frac{Mn}{6} + \frac{(Cr+Mo+V)}{5} + \frac{(Ni+Cu)}{15}$$

† Ito–Bessyo equivalent (P_{cm}) is given by[8]:

$$P_{cm} = C + \frac{(Mn+Cr+Cu)}{20} + \frac{Si}{30} + \frac{V}{10} + \frac{Mo}{15} + \frac{Ni}{60} + 5B$$

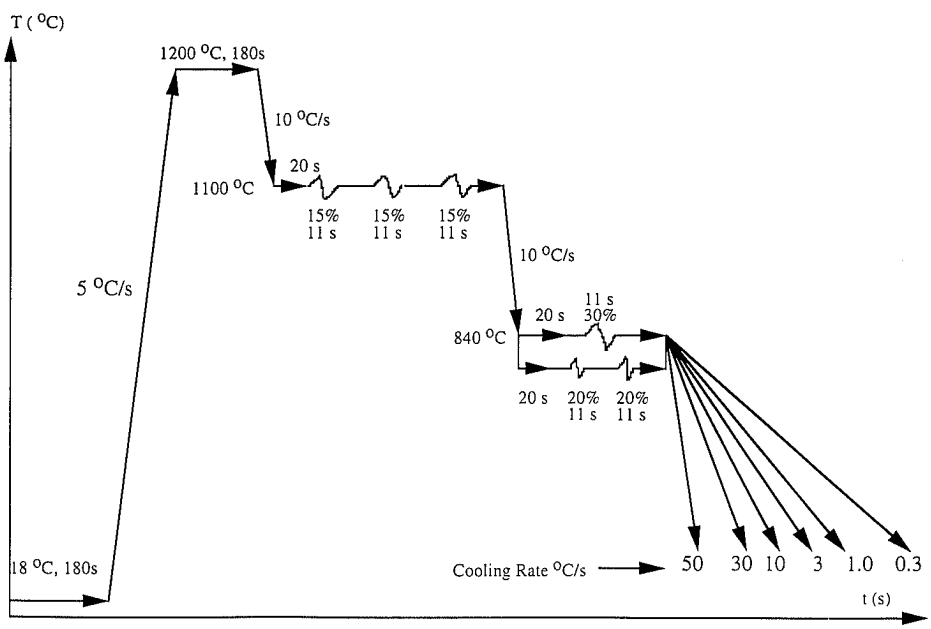

Fig. 1. Schematic presentation of the experimental program for dilatometry.

after the TMP using conventional techniques.

The schedule for deformation dilatometry is presented schematically in **Fig. 1**. The thermal cycle used for the undeformed samples was identical to that of deformed samples. Soaking temperature of 1 200°C ensured that most of the microalloying elements were in solution in austenite. Roughing rolling was simulated to some extent by giving three deformation passes of 15% reduction each at 1 100°C with an interpass time of 11 s. Austenite grain size after roughing deformation was similar in both steels (26.9 μm in Hi-Mn+Si steel and 26.5 μm in low-Mn+Si steel). Finishing deformation of either 30% (single pass) or 40% (two passes of 20% reduction in each pass) was given at 840°C to simulate controlled rolling practice for these steels. Finishing deformation temperature was chosen such that it was higher than the Ar_3 but well below "no recrystallization temperature (T_{nr})" to obtain a pancake microstructure in austenite after finishing deformation. Time of transformation was estimated from the dilation *v/s* time curve and was calculated as the time required for the transformation to progress from start to finish.

4. Results

Effect of cooling rate and TMP on γ transformation critical temperature, Ar_3, for Hi and low-Mn+Si steels is shown **Figs. 2** and **3** respectively. The results show that increase in cooling rate significantly lowers Ar_3 of undeformed and deformed samples in both steels. However, Ar_3 of deformed samples is higher than that of undeformed samples at similar cooling rates in both steels. For example, at a cooling rate of 0.3°C/s, in Hi-Mn+Si steel (Fig. 2), the Ar_3 temperature of undeformed, 30 and 40% finish deformed samples are found to be 720, 790 and 800°C respectively indicating the effect of TMP on the Ar_3 temperature.

Effect of cooling rate and TMP on the time of transformation is given in **Figs. 4** and **5** for Hi- and low-Mn+Si steels respectively. The data indicate that transformation time decreases as cooling rate is increased for both undeformed and deformed samples *i.e.* the progress of transformation becomes faster as the cooling rate increases. On the other hand, the time of transformation for the deformed samples is found to be longer as compared to that of samples in undeformed state with

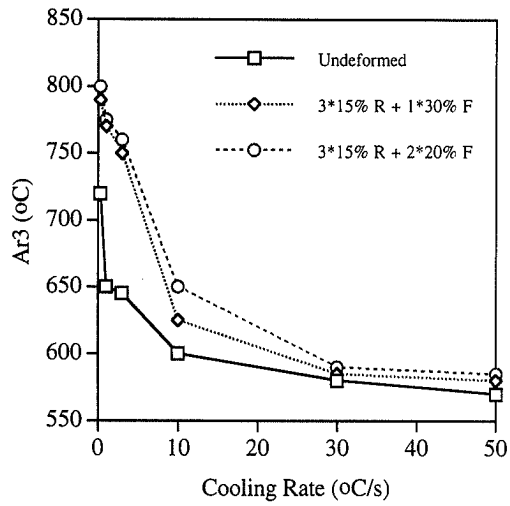

Fig. 2. Effect of cooling rate and TMP on Ar_3 for Hi-Mn+Si steel.

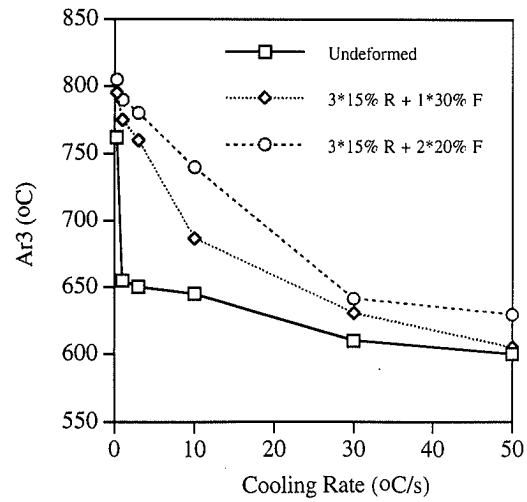

Fig. 3. Effect of cooling rate and TMP on Ar_3 for low-Mn+Si steel.

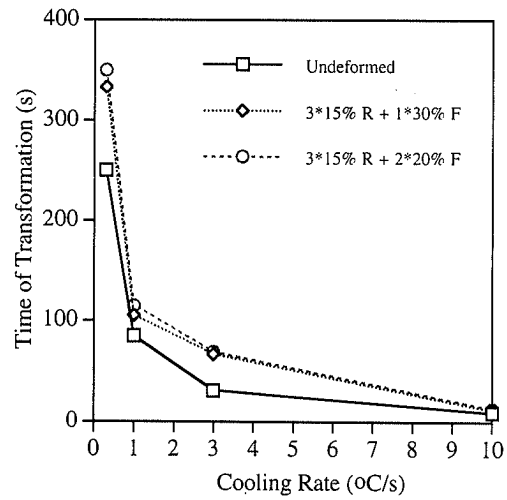

Fig. 4. Effect of cooling rate and TMP on the time of transformation for Hi-Mn+Si steel.

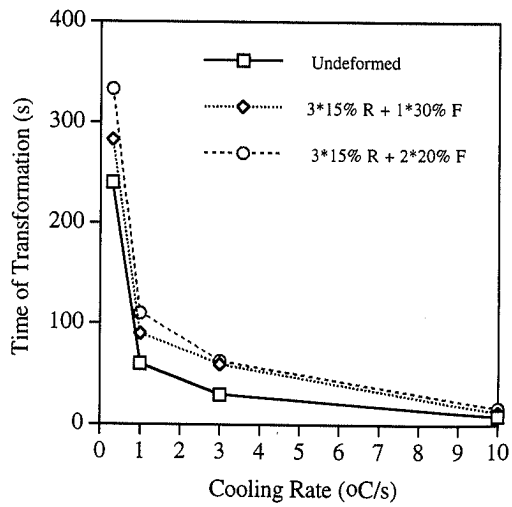

Fig. 5. Effect of cooling rate and TMP on the time of transformation for low-Mn+Si steel.

similar cooling rate in both steels. For example, at a cooling rate of 0.3°C/s in Hi-Mn+Si steel (Fig. 4), the transformation time for undeformed, 30 and 40% finish deformation samples are 250, 333 and 350 s respectively demonstrating that the progress of transformation is retarded by TMP.

Effect of Mn+Si content on Ar_3 and the time of transformation is presented in **Figs. 6** and **7** respectively. The results given in Fig. 6 show that the Ar_3 of Hi-Mn+Si is lower than that of low-Mn+Si steel in undeformed as well as deformed condition for all cooling rates used. It can be seen from Fig. 7 that the progress of transformation is sluggish in Hi-Mn+Si steel as compared to low-Mn+Si steel for all cooling rates used in undeformed condition and also in deformed condition except at 10°C/s. The reason for this will be explained later.

CCT diagrams for Hi-Mn+Si steel are presented in **Figs. 8–10** while CCT diagrams for low-Mn+Si steel are given in **Figs. 11–13**. Microconstituents are identified according to the classification system suggested by Bramfitt and Speer.[9] Typical optical microstructures at different cooling rates in Hi-Mn+Si steel are shown in **Fig. 14**. The microstructure of the undeformed sample cooled at 1°C/s (Fig. 14(a)) consists of widmanstatten ferrite and pearlite (B_3^P) with some polygonal ferrite while that of the deformed sample at the same cooling rate exhibits grain refined polygonal ferrite and pearlite. At a cooling rate of 10°C/s in undeformed samples, the microstructure is mainly upper bainite (B_2^c) while the deformed sample shows granular bainite (martensite–austenite islands distributed evenly within the matrix of acicular ferrite–B_3^{m-a}) with some polygonal ferrite (Fig. 14(b)). Lower bainite (B_1^c) is the predominant microstructure in the undeformed sample cooled at 50°C/s whilst the deformed sample exhibits upper bainite

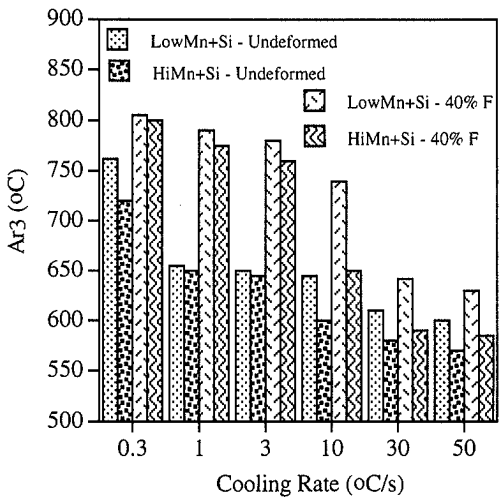

Fig. 6. Effect of composition (Mn+Si contents) on Ar_3 temperature.

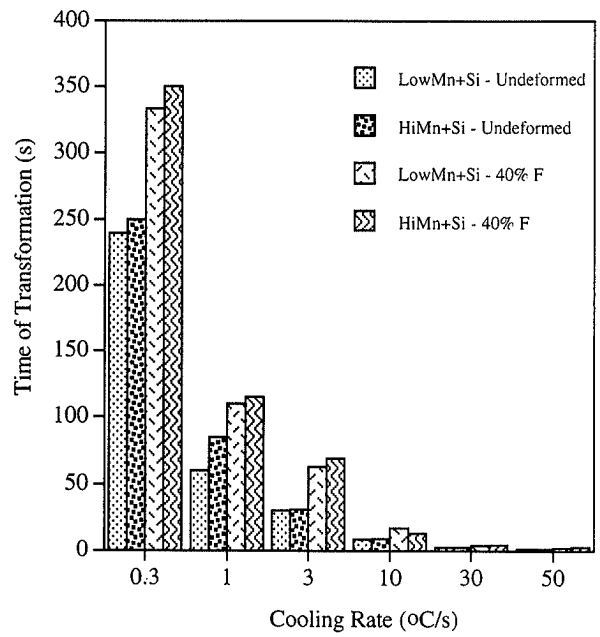

Fig. 7. Effect of composition (Mn+Si contents) on the time of transformation.

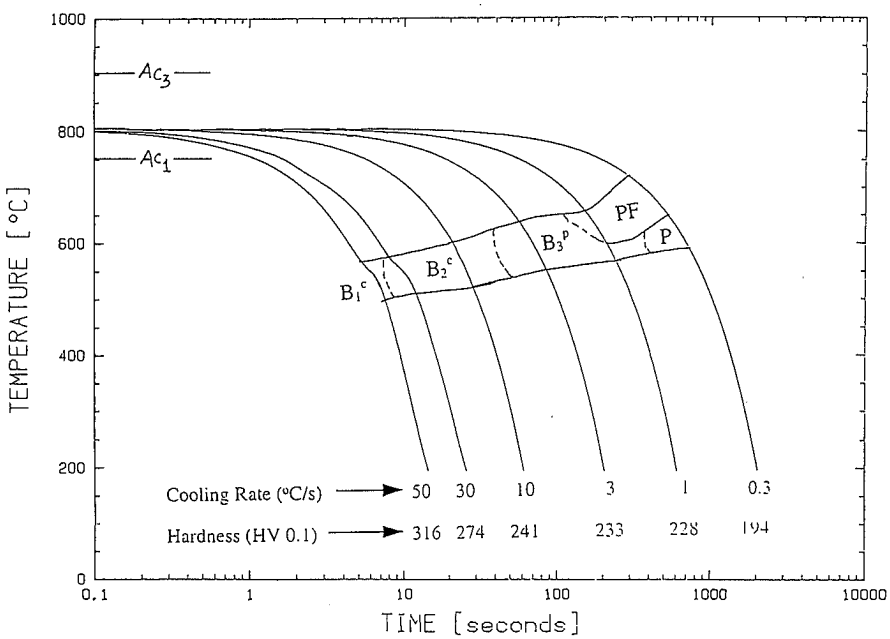

Fig. 8. CCT diagram for Hi-Mn+Si steel in undeformed condition.

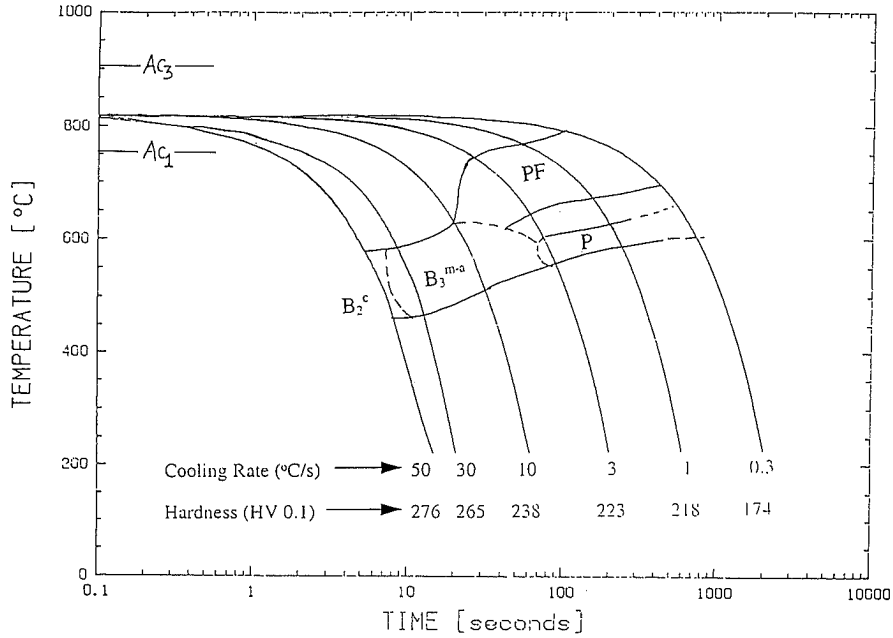

Fig. 9. CCT diagram for Hi-Mn+Si steel in deformed condition (3.15% roughing+1.30% finishing deformation).

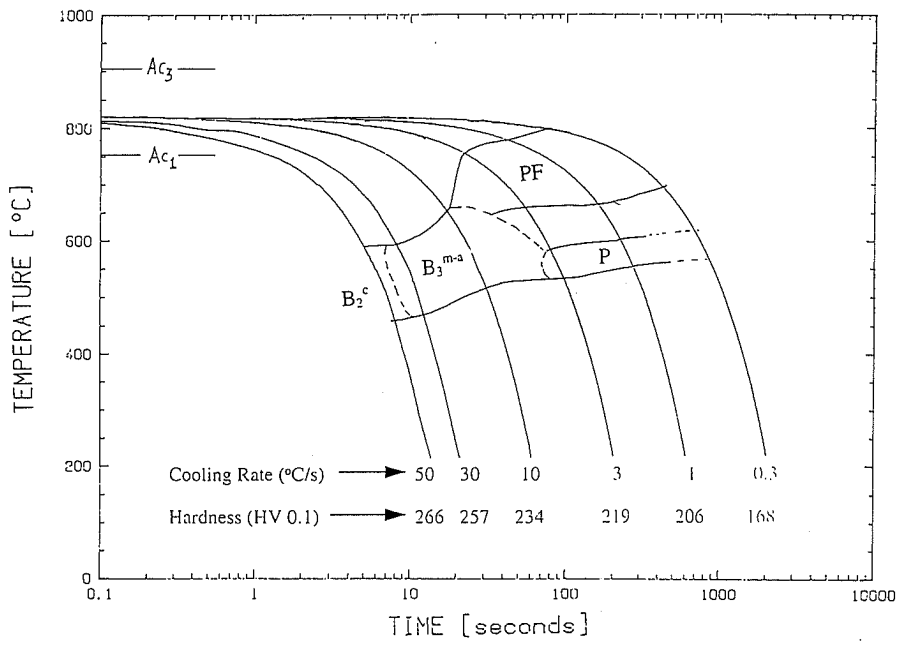

Fig. 10. CCT diagram for Hi-Mn+Si steel in deformed condition (3.15% roughing+2.20% finishing deformation).

with some martensite–austenite islands (Fig. 14(c)).

Comparison of CCT diagrams of the undeformed and deformed samples suggests the following:

(a) γ/α transformation is raised to higher temperatures indicating decreased hardenability of TMP austenite,

(b) ferrite transformation nose is shifted to higher cooling rates in deformed samples; and

(c) γ/α transformation occurs over a wider temperature range indicating a retarded rate of progress of transformation.

Effect of Mn+Si content on the CCT behaviour of the two steels can be seen by comparing the CCT diagrams given in Figs. 8–13. It can be seen from Figs. 9 and 10 that granular bainitic microstructure (B_3^{m-a}) is predominant at a cooling rate of 10°C/s in Hi-Mn+Si steel. On the other hand, in low-Mn+Si steel this microstructure is predominant only when the cooling rate is close to 30°C/s and polygonal ferrite continues to form until 30°C/s. This is the reason why the transformation kinetics of low-Mn+Si steel are slower than that of Hi-Mn+Si steel in deformed condition at 10°C/s. When comparable microstructures are produced in the two steels, the transformation kinetics of Hi-Mn+Si steel are slower than that of low-Mn+Si steel. Thus it is clear from Figs. 8–13 that the location of polygonal ferrite nose is significantly influenced by the Mn+Si contents and the TMP: TMP moves the PF nose towards left

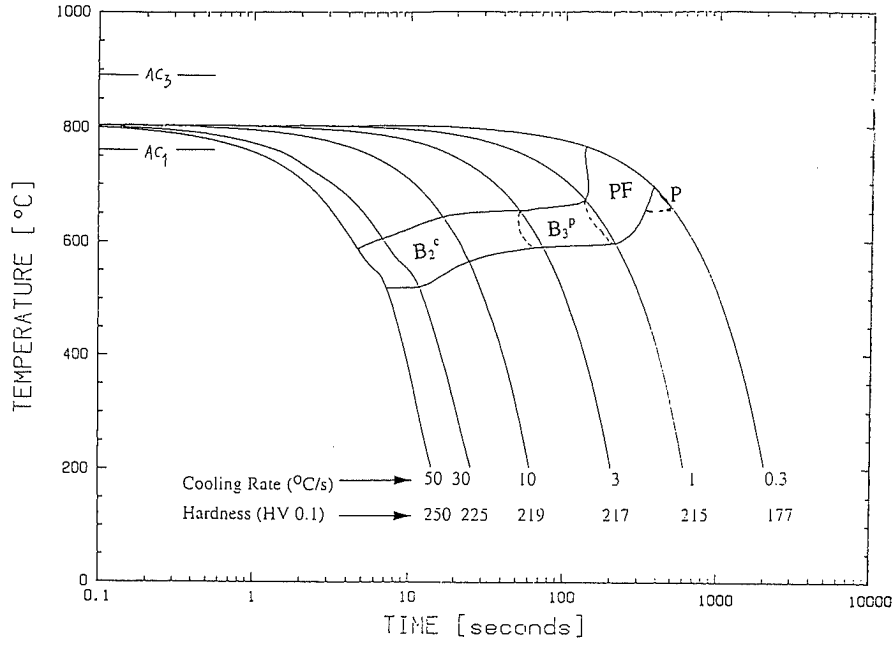

Fig. 11. CCT diagram for low-Mn+Si steel in undeformed condition.

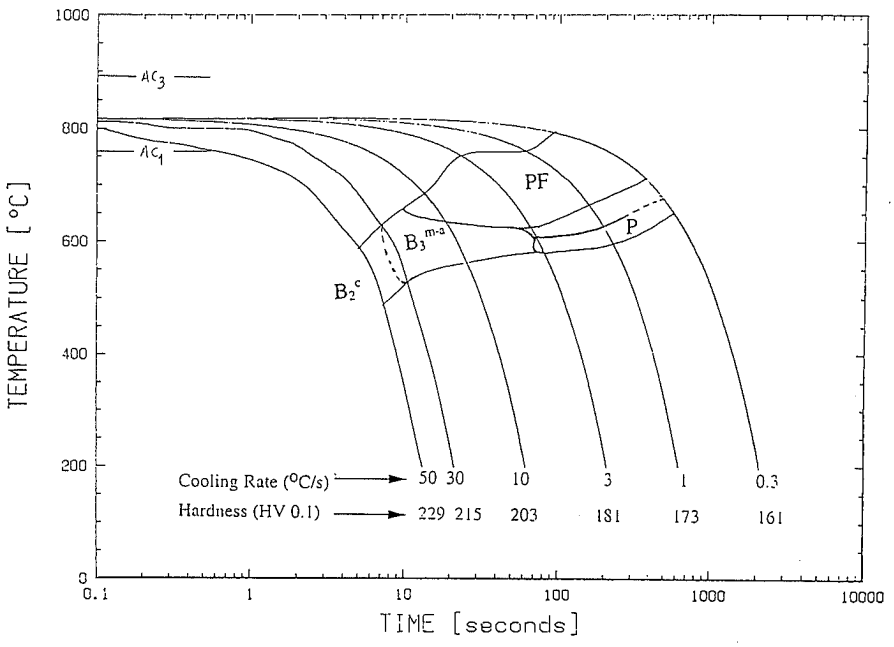

Fig. 12. CCT diagram for low-Mn+Si steel in deformed condition (3.15% roughing+1.30% finishing deformation).

(lowered hardenability) while a higher Mn+Si content pushes it to the right (increased hardenability).

5. Discussion

5.1. Effect of Mn+Si Content on γ/α Transformation

It is known that Mn dissolves in austenite and increases the hardenability of austenite as shown by its effect on the isothermal transformation diagrams. In the context of microalloyed steels, it has been suggested that increase in Mn content delays the precipitation of Ti,[10] and Nb[11,12] and increases the solubility of NbC by decreasing the diffusivity of Nb in austenite.[13] Mn lowers the Ar_3 temperature,[14-16] and suppresses or delays the γ/α transformation.[15,17-19] Addition of Mn has been found to:

- increase both nucleation and growth times during isothermal transformation of austenite,[20]
- decrease the activity of carbon in austenite[21] which leads to a hindrance to bainitic transformation and the promotion of the formation of MA constituents; and
- decrease austenite transformation kinetics through a strong solute drag like effect by segregating at austenite grain boundaries.[20,22,23]

On the other hand, the effect of Si addition on austenite transformation may or may not be additive to those due to Mn addition. Addition of Si decreases the solubility of NbC in austenite in microalloyed steels by increasing the diffusivity of Nb in austenite.[13] It has been shown that an addition of Si:

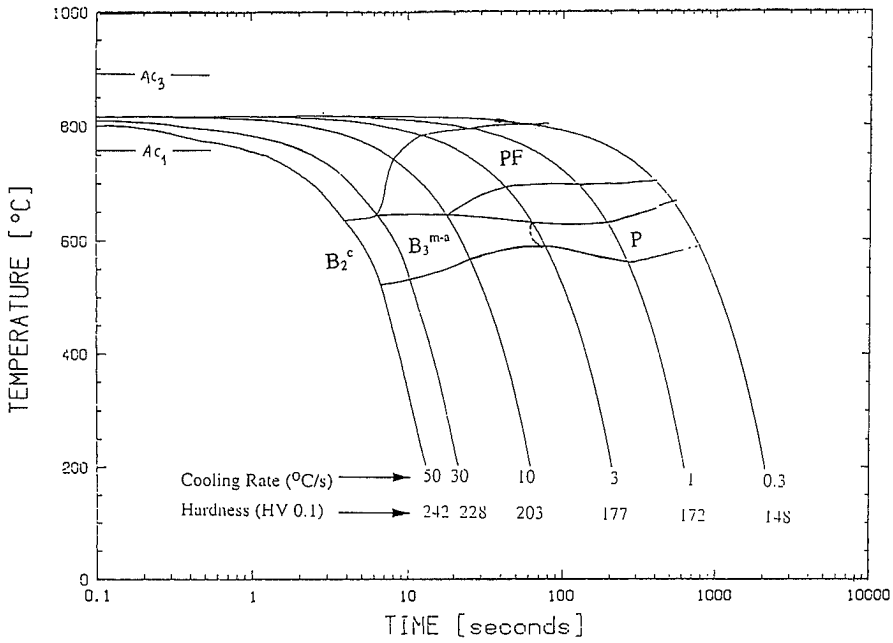

Fig. 13. CCT diagram for low-Mn+Si steel in deformed condition (3.15% roughing+2.20% finishing deformation).

• promotes transformation kinetics of grain boundary allotriomorphs of pro-eutectoid ferrite,[24] but Si prevents carbon from precipitating and therefore austenite gets enriched in carbon which reduces the driving force for sympathetic nucleation of the subsequent ferrite plates during bainitic transformation and thus may decrease the overall transformation kinetics of bainite in combination with Mn,[25]

• increases activity of carbon in austenite, however also hinders the precipitation and diffusion-controlled growth of carbides by forming a Si-enriched layer around precipitate nuclei[26] and thus hinders bainitic transformation and promotes the formation of MA constituents[5]; and

• enhances the segregation of Mn at austenite grain boundaries due to its negative interaction coefficient with carbon and thus reduces transformation kinetics of austenite due to an inverse solute drag effect.[20]

Thus, addition of Si has opposite effects to those due to Mn addition on the activity of carbon and diffusivity of Nb in austenite. On the other hand, other effects of Si addition such as increasing the hardenability and reducing transformation kinetics of austenite are similar to those due to Mn addition. The results obtained in the present work during continuous cooling transformation behaviour of Ti-bearing microalloyed steels seem to corroborate the previously reported effects during isothermal transformation. It can be observed from Figs. 6 and 7 that Hi-Mn+Si steel exhibits lowered Ar_3 temperature and sluggish transformation kinetics of austenite as compared to the low-Mn+Si steel. These effects can be explained in terms of higher Mn content which would lower Ar_3 and higher content of Mn and Si which contribute towards retardation of transformation kinetics in Hi-Mn+Si steel. Further, granular bainite (B_3^{m-a}) constituent can be seen to be a predominant phase transformation product in Hi-Mn+Si steel between 3–50°C/s cooling rates in deformed samples (Figs. 9 and 10). This results indicates that the addition of Mn and Si promotes the formation of granular bainite during continuous cooling transformation of thermomechanically processed microalloyed austenite. Polygonal ferrite nose is shifted to right from 30°C/s in low-Mn+Si steel (Fig. 13) up to 10°C/s in Hi-Mn+Si steel (Fig. 10) indicating increased hardenability of Hi-Mn+Si steel. Hi-Mn+Si steel also exhibits higher microhardness values in equivalent deformation and cooling conditions as compared to low-Mn+Si steel (Figs. 8–13).

5.2. Effect of TMP and Cooling Rate on γ/α Transformation

TMP has been found to retard the progress of γ/α transformation in both steels while increase in cooling rate accelerates it (Figs. 4 and 5). These observations have been reported and discussed in detail previously.[27,28] The reasons why deformed samples exhibit slower transformation kinetics are suggested to be due to lessening of driving force for transformation as the transformation progresses,[29] higher volume of material which must transform *via* intragranular nucleation,[30] pinning of interphase interface due to precipitation,[31] reduction of growth rate relative to nucleation due to strain induced precipitation.[32] A further reason could be that the very significant amount of pro-eutectoid ferrite transformation from TMP austenite would cause a higher carbon enrichment of the remaining austenite and thus stabilising it leading to the lowered rate of further transformation from the carbon enriched austenite. It would thus be expected that reaction kinetics would be retarded as the transformation progresses. This can be seen from the data given in **Fig. 15** which shows the progress of transformation in Hi-Mn+Si steel in undeformed and deformed conditions at cooling rates of 0.3 and 1°C/s. It is evident from these results that the

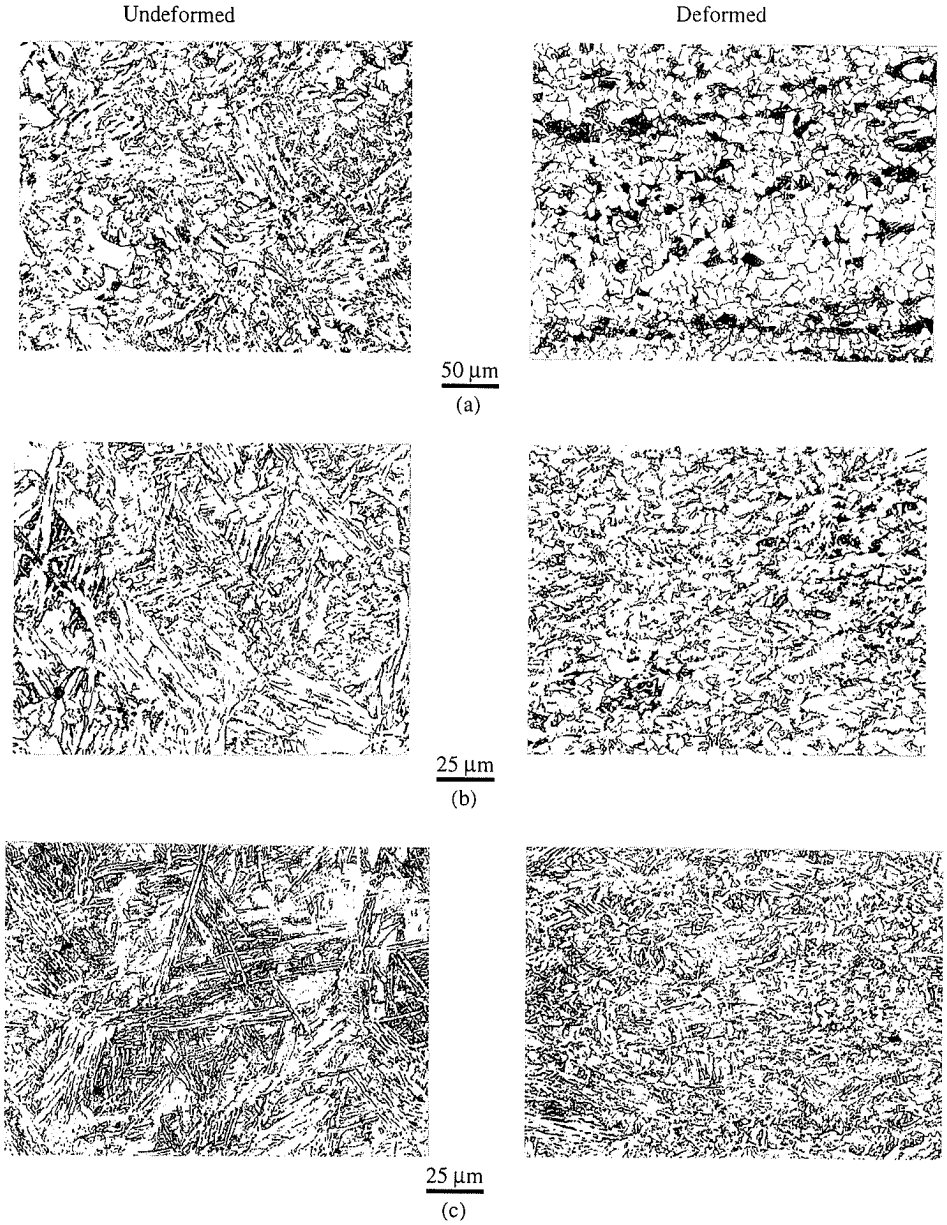

Fig. 14. Optical microstructures of the undeformed and deformed samples (3.15% R+2.20% F) in Hi-Mn+Si steel. The samples were cooled to room temperature after TMP at: (a) 1°C/s, (b) 10°C/s and (c) 50°C/s. See text for explanation. Etchant: 2.5% Nital.

progress of transformation in deformed samples is at least as rapid as that in undeformed samples until about 70% of the transformation is complete. However, the progress of the remaining final 30% of the transformation requires considerably longer time in deformed samples as compared to undeformed ones resulting in the net retardation of transformation in TMP samples. Similar results were obtained for the low-Mn+Si steel as well.

Another consequence of increased amount of pro-eutectoid ferrite in the microstructures of the deformed samples is the reduction in the hardness of samples as compared to undeformed samples at equivalent cooling rates (Figs. 8–13). Increased cooling rate lowers the Ar_3 (Figs. 2 and 3) leading to increased undercooling ($\Delta T = Ac_3 - Ar_3$) which increases the nucleation rate and also promotes intragranular nucleation. Further, increased cooling rate decreases the amount of pro-eutectoid ferrite that can form during transformation (because of suppression of growth rate of ferrite) and as a consequence the time of transformation is reduced.

6. Conclusions

(1) Effects of Mn+Si content on the CCT diagrams of the steels studied show that a higher Mn+Si content:

(a) lowers the Ar_3,
(b) increases the hardenability of undeformed and TMP austenite and pushes the polygonal ferrite nose towards right,
(c) promotes the formation of granular bainite (B_3^{m-a}) in deformed samples,
(d) reduces transformation kinetics; and
(e) increases the hardness of undeformed and deformed samples.

(2) Effect of TMP on the CCT diagrams of the steels

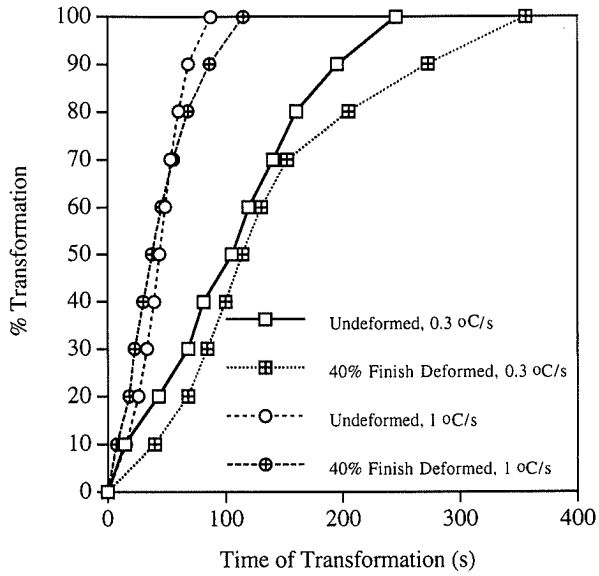

Fig. 15. Effect of TMP on the progress of transformation in Hi-Mn + Si steel.

studied show that:

(a) γ/α transformation is raised to higher temperatures indicating decreased hardenability of TMP austenite,

(b) polygonal ferrite nose if pushed towards left; and

(c) γ/α transformation occurs over a wider temperature range indicating retardation of the progress of transformation.

(3) Increase in cooling rate lowers the Ar_3, accelerates the progress of γ/α transformation and increases hardness in both steels.

Acknowledgements

The authors acknowledge the Australian Research Council for financial support and the BHP Steel Company, Port Kembla, Australia for providing experimental materials used in this work. Special thanks are due to Mr. Chris Killmore (BHP Steel, Port Kembla, Australia–Flat Products Division) and Dr. Kazutoshi Kunishige (Sumitomo Metal Industries Ltd., Japan–Sheet Products Research Department) for useful suggestions.

REFERENCES

1) J. G. Williams, C. R. Killmore, F. J. Barbaro, A. Meta and L. Fletcher: Proc. of Int. Conf. on Microalloying '95, ed. by M. Korchynsky *et al.*, ISS, Pittsburgh, (1995), 117.
2) B. de Meester: *ISIJ Int.*, **37** (1997), 537.
3) M. Korchynsky: Proc. of Int. Conf. on Microalloying '95, ed. by M. Korchynsky *et al.*, ISS, Pittsburgh, (1995), 3.
4) O. Grong and D. K. Matlock: *Int. Met. Rev.*, **31** (1986), 27.
5) R. Taillard, P. Verrier, T. Maurickx and J. Foct: *Metall. Trans. ASM*, **26A** (1995), 447.
6) J. L. Lee and Y. T. Pan: *Mater. Sci. Technol.*, **8** (1992), 236.
7) J. Dearden and H. O'Neill: *Trans. Inst. Weld.*, **3** (1940), 203.
8) Y. Ito and K. Bessyo: IIW Doc. IX-576-68.
9) B. L. Bramfitt and J. G. Speer: *Metall. Trans. ASM*, **21A** (1990), 817.
10) Z. Hongtao: Proc. of Int. Conf. on Microalloying '95, ed. by M. Korchynsky *et al.*, ISS, Pittsburgh, (1995), 61.
11) M. G. Akben, I. Weiss and J. J. Jonas: *Acta Metall.*, **29** (1981), 111.
12) L. Xiuqiu and C. Wenxuan: Proc. of Int. Conf. on HSLA Steels: Metallurgy and Applications, ed. by J. M. Gray *et al.*, Beijing, (1985), 235.
13) S. Kurokawa, J. E. Ruzzante, A. M. Hey and F. Dyment: *Met. Sci. J.*, **17** (1983), 433.
14) C. Ouchi, T. Sampei and I. Kozasu: *Trans. Iron Steel Inst. Jpn.*, **22** (1982), 214.
15) R. W. Honeycombe: Proc. of Int. Conf. on Processing, Microstructure and Properties of HSLA Steels, ed. by A. J. DeArdo, TMS, (1988), 1.
16) M. Cohen and S. S. Hansen: Proc. of Int. Conf. on HSLA Steels: Metallurgy and Applications, ed. by J. M. Gray *et al.*, Beijing, (1985), 61.
17) L. Meyer, F. Heisterkamp and W. Mueschenborn: Proc. of Int. Symp. Microalloying '75, Union Carbide Corp., Washington D.C., (1975), 153.
18) R. Priestner and M. S. Biring: *Met. Sci. J.*, **7** (1973), 60.
19) T. G. Oakwood, A. P. Coldren and K. Miyano: Proc. of Int. Conf. on HSLA Steels: Metallurgy and Applications, ed. by J. M. Gray *et al.*, Beijing, (1985), 715.
20) S. K. Liu and G. Y. Zhang: *Metall. Trans. ASM*, **21A** (1990), 1509.
21) J. S. Kirkaldy, B. A. Thomson and E. A. Baganis: Proc. Int. Symp. Hardenability Concepts with Applications to Steel, ed. by D. V. Doane and J. S. Kirkaldy, Met. Soc. AIME, Warrendale, PA, (1978), 82.
22) S. K. Liu and J. Zhang: *Metall. Trans. ASM*, **21A** (1990), 1517.
23) H. J. Grabke, K. Hennesen, R. Moller and W. Wei: *Scr. Metall.*, **21** (1987), 1329.
24) G. J. Shiflet, H. I. Aaronson and J. R. Bradley: *Metall. Trans. ASM*, **12A** (1981), 1743.
25) W. T. Reynolds, Jr., S. K. Liu, F. Z. Li, S. Hartfield and H. I. Aaronson: *Metall. Trans. ASM*, **21A** (1990), 1479.
26) H. K. D. H. Bhadeshia and D. V. Edmonds: *Metall. Trans. ASM*, **10A** (1979), 895.
27) P. A. Manohar, T. Chandra and C. R. Killmore: *ISIJ Int.*, **36** (1996), 1486.
28) P. A. Manohar and T. Chandra: Proc. of Int. Conf. on Thermomechanical Processing of Steels and Other Materials–THERMEC '97, Wollongong, Australia, ed. by T. Chandra and T. Sakai, TMS, (1997), 749.
29) X. Liu, J. K. Solberg and R. Gjengedal: Proc. of Int. Conf. HSLA '95, ed. by L. Guoxun *et al.*, Beijing, (1995), 253.
30) A. Sandberg and W. Roberts: Proc. of Int. Conf. on Thermomechanical Processing of Microalloyed Austenite, ed. by A. J. DeArdo *et al.*, AIME, (1982), 405.
31) R. W. K. Honeycombe: Proc. of Int. Conf. on HSLA Steels: Metallurgy and Applications, ed. by J. M. Gray *et al.*, Beijing, (1985), 243.
32) C. M. Sellars: Proc. of Int. Conf. on HSLA Steels: Metallurgy and Applications, ed. by J. M. Gray *et al.*, Beijing, (1985), 73.